Mixing Efficiencies in Patchy Turbulence

LARS ARNEBORG

Department of Oceanography, Earth Sciences Centre, Göteborg University, Goteborg, Sweden

ABSTRACT

The efficiency of mixing in stably stratified systems where the turbulent mixing is confined to intermittent patches is investigated theoretically. It is possible to define two different flux Richardson numbers for mixing in such a system. One, the small-scale flux Richardson number, R_{fi}, is based on the initial potential energy increase caused by small-scale turbulent mixing within the patches. This is the parameter that is obtained from laboratory and numerical experiments intended to determine turbulent mixing efficiencies. The other, the large-scale flux Richardson number, R_f, is based on the final potential energy increase, obtained after the mixed fluid has spread out laterally in the system. This is the relevant parameter for determining large-scale, irreversible, changes in the stratification caused by mixing. It is shown that the large-scale flux Richardson number is always smaller than the small-scale flux Richardson number, and that the difference can be almost a factor of 2.

The commonly used mixing efficiencies, 0.17–0.2, obtained from laboratory and numerical experiments of small-scale homogeneous turbulence, are a measure for the small-scale flux Richardson number R_{fi} rather than the large-scale flux Richardson number R_f. If the maximum small-scale flux Richardson number $R_{fi} = 0.2$ is relevant for mixing in oceanic patches, one should use $R_f = 0.11$ for the large-scale flux Richardson number. The latter value is supported by results from recent microstructure experiments in the ocean.

1. Introduction

There appears to be some confusion about which values to use for mixing efficiencies in stably stratified geophysical turbulence. On one side, the community of oceanographers who measure turbulent kinetic energy dissipation seem to have reached consensus in using flux Richardson numbers[1] in the range $R_f = 0.17$–0.20 when estimating the turbulent diffusion coefficient, K_z, from measured values of the dissipation rate, ϵ, of turbulent kinetic energy (e.g., Ledwell et al. 2000 and Inall et al. 2000). On the other hand, oceanographers who have obtained the mixing efficiencies from energy budgets in stagnant fjord basins reach values as small as $R_f \approx 0.06$–0.07 (e.g., Stigebrandt 1999; Arneborg and Liljebladh 2001).

The larger values for the mixing efficiencies seem to be supported by laboratory experiments (Linden 1979; Rohr et al. 1984; Piccirillo and Van Atta 1997) and direct numerical simulations (Itsweire et al. 1993) of

turbulence under stably stratified conditions. These experiments indicate that the flux Ricardson number varies in the range 0–0.2, and that the maximum value, 0.2, is obtained at a critical turbulent Froude number. Field data from lakes (Imberger and Ivey 1991) indicate that turbulent Froude numbers in the interior of lakes are often close to the critical value. This seems to support the use of a flux Richardson number close to 0.2.

In the ocean, mixing efficiencies have mainly been estimated from microstructure measurements. In such measurements the vertical buoyancy flux has been estimated from temperature microstructure using the Osborn and Cox (1972) model (hereafter the OC model), while ϵ has been estimated from velocity microstructure. Early such estimates have given flux Richardson numbers in the range $R_f = 0$–0.29; see Ruddick et al. (1997) for a review. The main problem with many of these measurements is that buoyancy fluxes caused by double-diffusive processes have not been separated from buoyancy fluxes caused by active turbulent mixing.

In a recent study St. Laurent and Schmitt (1999) were able to separate their ocean mixing efficiency estimates into bins with regard to the stability parameter R_ρ, defined as

$$R_\rho \equiv \frac{\alpha \theta_z}{\beta S_z}, \qquad (1)$$

and the gradient Richardson number, Ri, defined as

---

[1] I have chosen mainly to use the flux Richardson number, R_f, rather than the mixing ratio, Γ, as representation for the mixing efficiency. The two mixing efficiencies are related through $R_f = \Gamma(1 + \Gamma)^{-1}$ (e.g., St. Laurent and Schmitt 1999).

Corresponding author address: Dr. Lars Arneborg, Department of Oceanography, Göteborg University, Box 460, Göteborg 40530, Sweden.
E-mail: laar@oce.gu.se

$$\text{Ri} \equiv \frac{N^2}{U_z^2}, \tag{2}$$

where $-\alpha\theta_z$ is the temperature contribution and βS_z is the salinity contribution to the normalized vertical density gradient, N is the buoyancy frequency, and U_z is the vertical gradient of the finescale (based on 5-m segments) horizontal velocity. Considering only the part of their data dominated by stably stratified turbulence ($R_\rho < 0$, Ri < 1; see their Fig. 8, panel c), one obtains an average mixing ratio $\Gamma = 0.12$ (corresponding to $R_f = 0.11$). This result is based on about 17.000 microstructure segments! This is to my knowledge the most thorough and accurate oceanic mixing efficiency estimate till date.

As oceanographers we are mainly interested in the large-scale changes in stratification, caused by turbulent mixing. When wanting to apply the results above to estimate large-scale changes of stratification in the ocean, two questions arise: (i) Do the small-scale laboratory experiments describe all processes involved in oceanic mixing, and (ii) can the OC model be used to deduce large-scale mixing from temperature microstructure? The latter question has been treated formally by Winters and D'Asaro (1996), who introduce a more correct procedure to determine irreversible diapycnal mixing. They do not discuss, however, when one may expect the OC model to work and when not, and how wrong the results may be.

In laboratory and numerical experiments the turbulence is often relatively homogeneously distributed over the tank/model domain. In real geophysical systems, however, turbulence is extremely patchy and intermittent (e.g., Gregg 1998). In a patchy mixing event, a certain amount of potential energy is gained by the initial turbulent mixing within the patch. Such a patch has a length scale in the order of 1–10 m, that is, the same length scale as a typical tank, and it is reasonable to assume that the turbulence within the patch is relatively homogeneous, as it is in most tank experiments. It is therefore also reasonable to assume that tank experiments give a good representation of this initial mixing. After the turbulence within the patch has faded away, the mixed fluid within the patch will tend to collapse laterally. During the collapse, the patch will lose up to half of the initially gained potential energy, as noted by Garrett (1984) and recapitulated in section 2 of this paper. The mixing efficiency based on the final potential energy increase is therefore smaller than that based on the initial, turbulent mixing, as discussed in section 3. The collapse is not included in experiments focused on small-scale mixing, which means that one may expect large-scale mixing efficiencies to be smaller than those obtained from these experiments, as discussed further in section 4.

The use of the OC model in a patchy ocean is also discussed in section 4. It is not straightforward to use the OC model and the diapycnal flux model in Winters
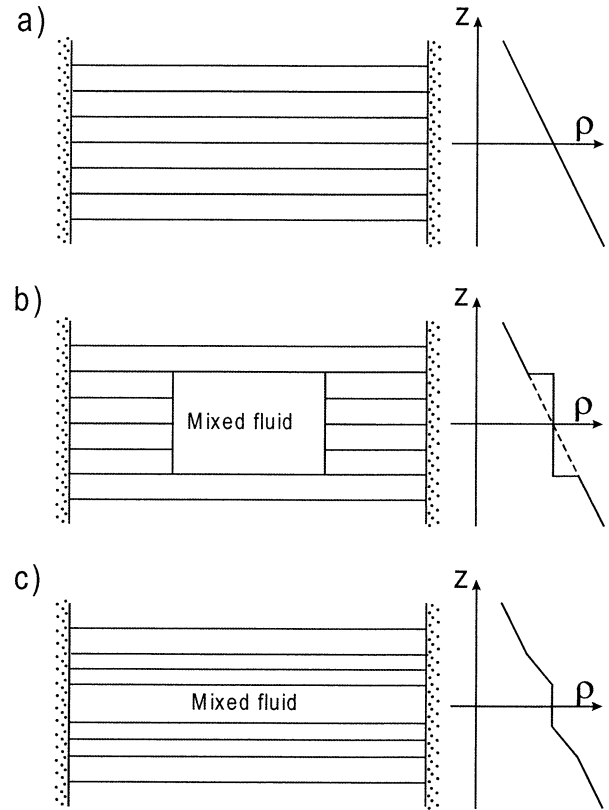

FIG. 1. Vertical section and density profile through (a) a linearly stratified basin (state A), (b) the same basin after total mixing of a patch (state B), and (c) after the mixed fluid has spread out into the whole basin (state C).

and D'Asaro (1996) in the case of patchy mixing. In section 5, I have posed two apparent paradoxes and their explanations, in order to obtain more experience with the models, and with the limitations of the OC model. The paper is concluded in section 6.

2. Patchy mixing

Following Garrett (1984), I consider the sequence of states shown in Fig. 1. An initially linearly stratified fluid (state A) is disturbed by a turbulent mixing event taking place within a finite patch. The turbulent mixing homogenizes the fluid within the patch, leading to state B. The change in potential energy from state A to state B is

$$\Delta E_{pAB} = \frac{1}{12} \rho_0 N_0^2 d^3 a, \tag{3}$$

where d is the thickness of the patch, a is the horizontal area of the patch, and N_0 is the buoyancy frequency of the background stratification.

At the lateral boundaries of the mixed patch there are lateral pressure gradients, which will make the patch tend to collapse, losing some of the gained potential energy. In the absence of viscosity it will spread out to

its internal Rossby radius, but due to viscosity it will spread out even farther (Garrett 1984). After the patch has spread into the horizontal area A (state C, Fig. 1) the difference in potential energy from state A to state C is

$$\Delta E_{pAC} = \frac{1}{24}\rho_0 N_0^2 d^3 \left(1 + \frac{a}{A}\right)a, \qquad (4)$$

taking into account also the displacement of fluid outside the patch. Intuitively one would expect the patch to lose all potential energy if spreading out infinitely, but this is wrong. For an infinite spreading ($a/A \to 0$) the final potential energy gain is half the initial potential energy gain; that is, the patch loses half of the initial potential energy.

The difference in potential energy between state B and state C is going into kinetic energy in the intruding gravity current and into shear waves radiating away from the intruding patch (e.g., Lemckert and Imberger 1993; De Silva and Fernando 1998). This is in turn transferred into additional turbulence and mixing. The final potential energy increase caused by the mixing event is therefore slightly larger than that of state C, as discussed further in section 3.

If the initial turbulence is not able to completely homogenize the fluid within the patch, the stratification within the patch will reach gravitational equilibrium with the surrounding stratification before the patch has spread out into the whole basin. In that case the difference between the potential energies at state B and C is smaller than that expressed by (3) and (4). This problem was solved by Hebert (1988), and is recapitulated in the appendix.

Turbulent patches may be oblique, rather than horizontal, if for example the turbulence is caused by breaking of internal waves within an internal wave group (Thorpe 1999) or if the turbulence is caused by breaking of an internal wave at a sloping bottom (Garrett 1991). A similar analysis as above can be done for such patches. If the patch is much smaller than the basin, one obtains the same result as for the horizontal patch: the potential energy increase from state A to state C is half the potential energy increase caused by the initial mixing (state A to state B; see Garrett 1991).

3. Mixing efficiencies

In a closed system without buoyancy fluxes across the boundaries, the rate of change in potential energy, ignoring molecular diffusion, is given by (e.g., Winters et al. 1995)

$$\frac{\partial E_p}{\partial t} = \int_V g\rho w \, dV, \qquad (5)$$

where V is the volume of the system.

An often used definition of the flux Richardson number (e.g., Ivey and Imberger 1991) is as the production of potential energy by vertical buoyancy fluxes divided by the loss of kinetic energy to dissipation and potential energy; that is,

$$R_f = \frac{g\langle\rho'w'\rangle}{\rho_0\varepsilon + g\langle\rho'w'\rangle}, \qquad (6)$$

where angle brackets denote mean values while the primes denote the corresponding fluctuating components. Note that only the changes in potential energy due to transports by the fluctuating components are included in this definition. Transports by the mean flow are not included. The result therefore becomes dependent of the choice of averaging scale, as will be seen below.

Returning to the example in section 2, we start with defining the averaging time scale in (6) so that it is longer than a characteristic time scale for the turbulence but shorter than a characteristic timescale for the collapse. Similarly the averaging length scale is shorter than the height of the patch but larger than the largest turbulent motions. Between state A and B changes in the potential energy are only caused by the fluctuating components. By use of (5), Eq. (6) can be rewritten as

$$R_{ft} = \frac{\Delta E_{pAB}}{\int_A^B \int_V \rho_0\varepsilon \, dV \, dt + \Delta E_{pAB}}, \qquad (7)$$

where index t is used to indicated that this flux Richardson number is related to small-scale, turbulent fluctuations.

If it is, however, chosen to use a much longer averaging timescale in (6), a timescale equal to the time difference between state A and state C, the countergradient buoyancy fluxes during the collapse are included into the fluctuating part of the motions. Now (6) can be written as

$$R_f = \frac{\Delta E_{pAC}}{\int_A^C \int_V \rho_0\varepsilon \, dV \, dt + \Delta E_{pAC}}. \qquad (8)$$

Where the small-scale flux Richardson number in (7) only represent the turbulent buoyancy fluxes, the large-scale flux Richardson number in (8) represent all buoyancy fluxes caused by the initial turbulence event, including the nonturbulent, countergradient fluxes taking place during the collapse. Ignoring the extra mixing and dissipation taking place between state B and C (it will be seen below why this can be done), the relation between the small-scale flux Richardson number, R_{ft}, and the large-scale flux Richardson number, R_f, can be found, using (3), (4), (7), and (8):

$$R_f = \frac{1 + aA^{-1}}{2 - (1 - aA^{-1})R_{ft}}R_{ft}. \qquad (9)$$

For $a/A = 1$, which means that the turbulence covers

the whole horizontal area, the two flux Richardson values are identical; that is, $R_f = R_{ft}$. This is the case that is most relevant for most experiments. In the limit of extreme patchiness, which is more relevant for the interior ocean, the fraction a/A can be taken as zero, which means that

$$\lim_{a/A \to 0} R_f = \frac{1}{2 - R_{ft}} R_{ft}. \qquad (10)$$

Inserting $R_{ft} = 0.2$ in (10), as an example, gives the large-scale flux Richardson number, $R_f = 0.11$.

Closing the energy budget

In the derivation of (9) the extra mixing and dissipation taking place during the collapse was ignored. In order to investigate the effect of these contributions and obtain a consistent energy budget, it is convenient to use the concepts of background potential energy, available potential energy, and diascalar flux, as introduced in Winters et al. (1995) and Winters and D'Asaro (1996).

The background potential energy, E_b, is defined as the minimum potential energy attainable through adiabatic redistribution of ρ (Winters et al. 1995). This can be written as

$$E_b = \int_V g\rho z^* \, dV, \qquad (11)$$

where z^* is the vertical position of each fluid parcel after adiabatic redistribution. The background potential energy can change due to diffusive and advective fluxes across the boundaries and by small-scale molecular diapycnal diffusion of density. In a closed basin the background potential energy can only change due to diapycnal diffusion of density; that is,

$$\frac{\partial E_b}{\partial t} = \int g\varphi_d A \, dz^*, \qquad (12)$$

where φ_d is the flux of density across an isopycnal surface per unit horizontal area (Winters et al. 1995).

The background potential energy at state B is the potential energy, obtained after adiabatic redistribution to static equilibrium. This is equal to the potential energy of state C in (4) calculated without taking into account the additional mixing taking place between state B and C. This means, using (3) and (4), that the change in background potential energy from state A to state B can be written as

$$\Delta E_{bAB} = \frac{1}{2}\left(1 + \frac{a}{A}\right)\Delta E_{pAB}. \qquad (13)$$

In the limit $a/A \to 0$ the background potential energy increase is only half the total potential energy increase.

The difference between the total potential energy and the background potential energy at state B is the available potential energy, E_a. This is the energy that can be
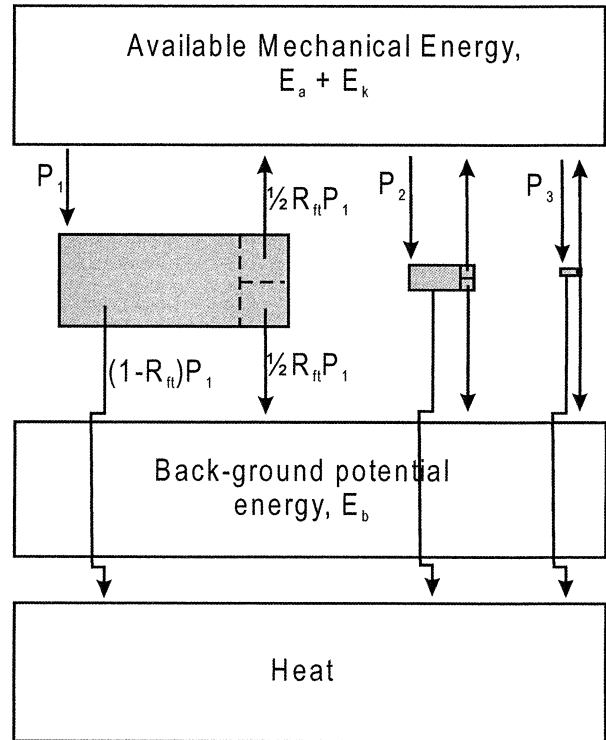

FIG. 2. Energy budget for a patchy mixing event. Of the initial turbulence production, P_1, most is lost to heat through dissipation. A small fraction is lost irreversibly to background potential energy. Another small fraction is put back into available mechanical energy. The latter amount of energy can be used to produce new turbulence, etc. The ratio of the total background potential energy increase to the initial turbulence production is given by the large-scale flux Richardson number in (15).

used to drive the intruding current and finally get lost to turbulence, dissipation, and additional mixing. In Fig. 2, I have sketched an energy budget for the case $a/A \to 0$. The initial production of turbulent kinetic energy, P_1, between state A and B, is taken from the available mechanical energy, which I define as the sum of the available potential energy and the nonturbulent kinetic energy. Most of this, $(1 - R_{ft})P_1$, is going into dissipation, the rest is used to increase the potential energy due to mixing within the patch. Half of the potential energy increase is lost irreversibly to background potential energy. The rest is available potential energy, which is put back into the available mechanical energy pool. The remaining available mechanical energy, $P_2 = \frac{1}{2}R_{ft}P_1$, can later be used to generate new turbulent patches. Again most of the energy going into these turbulent patches is lost to heat due to dissipation, while the rest is used to increase the potential energy. Only half of the potential energy increase is background potential energy increase, while the other half is put back into the available mechanical energy pool, etc.

The final, large-scale, flux Richardson number can now be determined from (8)

$$R_f = \frac{\Delta E_{b\mathrm{AC}}}{\int_A^C \int_V \rho_0 \varepsilon \, dV \, dt + \Delta E_{b\mathrm{AC}}}, \qquad (14)$$

where it has been used that $\Delta E_{p\mathrm{AC}} = \Delta E_{b\mathrm{AC}}$ since the available potential energy is zero at state A and C. From Fig. 2 we see, however, that the ratio between the background potential energy increase and the dissipation is the same in each patchy mixing event, which means that the final flux Richardson number can be written as

$$R_f = \frac{\sum_{i=1}^{\infty} \frac{1}{2} R_{ft} P_i}{\sum_{i=1}^{\infty} (1 - R_{ft}) P_i + \sum_{i=1}^{\infty} \frac{1}{2} R_{ft} P_i} = \frac{1}{2 - R_{ft}} R_{ft}. \quad (15)$$

It is seen that (15) is identical to (10). This illustrates that the additional mixing does not influence the results in (9) and (10), even though the final potential energy in state C is larger than that given in (4).

4. Relation between mixing efficiencies obtained in the laboratory, in numerical models, and in the ocean

In section 3 it was shown that it was possible to define two flux Richardson numbers for the same patchy mixing event. One, the small-scale flux Richardson number R_{ft}, defined through (7), was based on the initial turbulent mixing within the patch, while the other, R_f, defined through (8), was based on the final large-scale potential energy increase caused by the mixing. Since the two may differ with almost a factor of 2, it is important to evaluate different experimental methods in order to sort out, which of the two mixing efficiencies they can be expected to represent.

a. The relation between numerical and laboratory experiments and patchy mixing

The laboratory (e.g., Linden 1979 and Rohr et al. 1984) and numerical (e.g., Itsweire et al. 1993) results, which are used as arguments for the commonly used flux Richardson number, $R_f = 0.17$ (e.g., Ledwell et al. 2000), are all based on experiments of stationary, homogeneous turbulence. In these experiments the flux Richardson numbers are obtained from (6) by measuring time series of the turbulent fluctuations followed by time averaging.

All these experiments describe small-scale, relatively homogeneous, turbulence, covering most of the flume or numerical domain. None of them describe turbulence in a patch of finite horizontal extent with a following collapse. There may be some countergradient fluxes within the flume, but similarly may there be some countergradient fluxes within the turbulent patch during the initial mixing. These are part of the turbulence, and they are not organized large-scale flows as is the collapse of

a mixed patch. These experiments are aimed specifically at identifying characteristics of the small-scale turbulent fluctuations, not large-scale system parameters depending on the flume size. It therefore seems most reasonable that the results of the laboratory and numerical experiments represent R_{ft} rather than R_f.

If we therefore want to apply these results to estimate irreversible mixing in the ocean, we need to take into account the difference between R_{ft} and R_f described in the previous section. Assume that the value, $R_{ft} \approx 0.2$, is reasonable for the most energetic turbulent patches in the ocean. Then (15) gives the value, $R_f = 0.11$, for the large-scale flux Richardson number.

b. Mixing efficiencies obtained with the Osborn and Cox (1972) model

In order to obtain estimates for mixing efficiencies in the ocean, one needs to obtain estimates for both the dissipation of kinetic energy and for the vertical buoyancy flux. In the following we assume that the estimates of kinetic energy dissipation are correct. The estimate of vertical buoyancy fluxes in the oceans is less straightforward. One way to estimate vertical buoyancy fluxes is by using the OC model, which expresses a balance between the production of temperature variance and the dissipation, χ, of temperature variance by molecular diffusion; that is,

$$2\langle w'T' \rangle \left\langle \frac{\partial T}{\partial z} \right\rangle = -\chi. \qquad (16)$$

Introducing the definition of χ the vertical temperature flux can be written as

$$\langle w'T' \rangle = -\frac{\kappa_T \langle |\boldsymbol{\nabla} T|^2 \rangle}{\langle \partial T / \partial z \rangle}, \qquad (17)$$

where κ_T is the molecular diffusion coefficient for temperature.

After introducing turbulent diffusion coefficients for the vertical temperature flux,

$$K_T = -\frac{\langle w'T' \rangle}{\langle \partial T / \partial z \rangle}, \qquad (18)$$

and for the density flux

$$K_\rho = -\frac{\langle w'\rho' \rangle}{\langle \partial \rho / \partial z \rangle}, \qquad (19)$$

and assuming that these turbulent diffusion coefficients are identical, the vertical density flux can be written as

$$\langle w'\rho' \rangle = -\frac{\chi \langle \partial \rho / \partial z \rangle}{2 \langle \partial T / \partial z \rangle^2}. \qquad (20)$$

The mixing ratio, $\Gamma = R_f (1 - R_f)^{-1}$, can now by use of (6) be found as

$$\Gamma = \frac{g \langle w'\rho' \rangle}{\rho_0 \varepsilon} = \frac{\chi \langle N^2 \rangle}{2 \varepsilon \langle \partial T / \partial z \rangle^2}, \qquad (21)$$
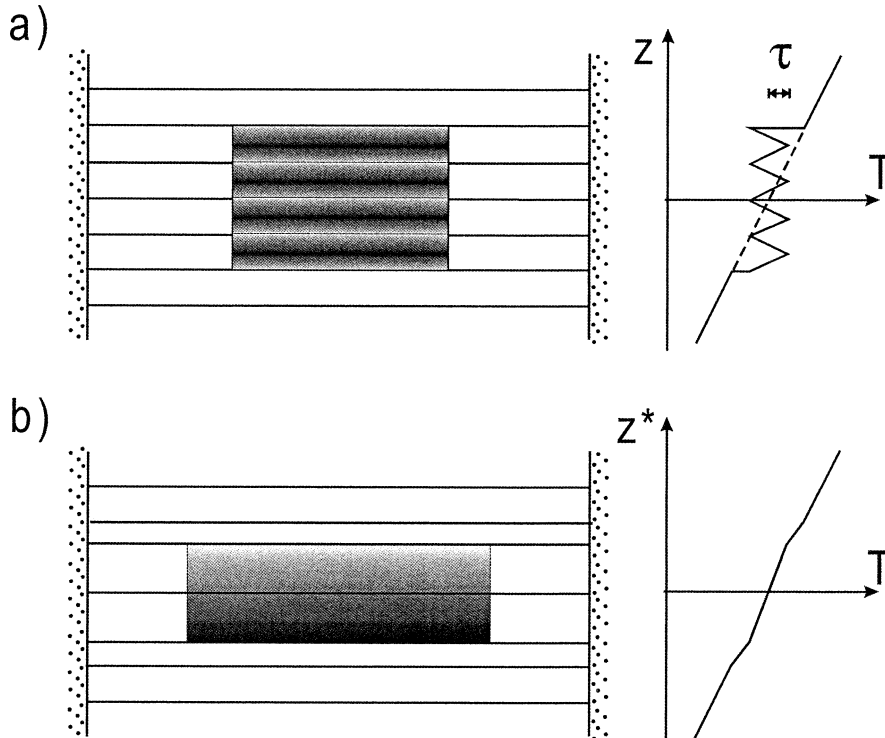
FIG. 3. Patch in a thermally stratified basin (a) before and (b) after redistribution to state of minimum potential energy.

which is the model used in, for example, St. Laurent and Schmitt (1999). In practice the average values, and the values of ϵ and χ, are obtained as averages over a large number of microstructure segments.

In order to evaluate the result of such a procedure, I will compare the rate of potential energy increase, obtained from (20) and (5), with the rate of background potential energy increase. The rate of background potential energy increase can be found from (12) if the diapycnal density flux, φ_d, is known. As shown in Winters and D'Asaro (1996) the diascalar flux, $\varphi_{d\theta}$, of some scalar, θ, can be written as

$$\varphi_{d\theta} = -\kappa_\theta \frac{dz^*}{d\theta} \langle |\nabla\theta|^2 \rangle_{z^*}, \qquad (22)$$

where κ_θ is the molecular diffusion coefficient, and $\langle \cdot \rangle_{z^*}$, denotes horizontal averaging, performed after adiabatic redistribution of all water parcels and their corresponding values of $|\nabla\theta|^2$. It is seen that the vertical temperature flux in (17) is very similar to the diascalar temperature flux obtained from (22) by replacing θ with T. The two fluxes are, however, not necessarily identical due to the differences in averaging, as discussed in Winters and D'Asaro (1996).

Consider a small patch in a large ocean. Assume that the water is only temperature stratified and that the temperature distribution within the patch at some time between state A and B (before complete homogenization) looks like illustrated in Fig. 3, while the water outside

the patch is linearly stratified. This is an unrealistic situation, but it is a possible situation, and it is convenient for our calculations. The mean-squared temperature gradient, calculated after the fluid has been redistributed, is

$$\langle |\nabla T|^2 \rangle_{z^*} = \frac{1}{A}\left[(A - a')\left(\frac{dT_0}{dz}\right)^2 + a'\left(\frac{2n\tau}{d}\right)^2\right],$$
$$-\frac{da}{2a'} < z^* < \frac{da}{2a'}, \qquad (23)$$

where n is the number of unstable density gradients within the patch, τ is the amplitude of the temperature perturbations, A is the basin area, a and d are the initial patch area and thickness, and a' is the horizontal area of the patch after adiabatic redistribution (Fig. 3). For $a/A \to 0$ corresponding to a large basin, and $a'(2n\tau/d)^2 \gg A(dT_0/dz)^2$ corresponding to much larger mixing within the patch than outside, one obtains

$$\langle |\nabla T|^2 \rangle_{z^*} = \frac{2a}{A}\frac{dT_0}{dz}\frac{n^2\tau}{d},$$
$$-\tau\left(\frac{dT_0}{dz}\right)^{-1} < z^* < \tau\left(\frac{dT_0}{dz}\right)^{-1}. \qquad (24)$$

The background temperature gradient for $a/A \to 0$ is

$$\frac{dT}{dz^*} = \frac{dT_0}{dz}. \qquad (25)$$

The diascalar flux of temperature is, from (22), (24), and (25),

$$\varphi_{dT} = -2\frac{a\kappa_T n^2 \tau}{Ad},$$

$$-\tau\left(\frac{dT_0}{dz}\right)^{-1} < z^* < \tau\left(\frac{dT_0}{dz}\right)^{-1}, \qquad (26)$$

which gives the diapycnal flux of density

$$\varphi_d = 2\frac{\alpha\rho_0 a\kappa_T n^2 \tau}{Ad},$$

$$-\tau\left(\frac{dT_0}{dz}\right)^{-1} < z^* < \tau\left(\frac{dT_0}{dz}\right)^{-1}, \qquad (27)$$

where α is the thermal expansion coefficient. The rate of change in background potential energy caused by diapycnal mixing within the patch is, using (12),

$$\frac{\partial E_b}{\partial t} = 4a\alpha g\rho_0\kappa_T n^2 \tau^2\left(d\frac{dT_0}{dz}\right)^{-1}. \qquad (28)$$

Returning to the OC expression in (17) for the vertical temperature flux, the basin-average vertical temperature gradient for $a/A \to 0$ is

$$\left\langle\frac{\partial T}{\partial z}\right\rangle = \frac{dT_0}{dz}, \qquad (29)$$

and for $a(2n\tau/d)^2 \gg A(dT_0/dz)^2$ the volume average temperature gradient variance over a horizontal slice of thickness D, enclosing the patch, is

$$\langle|\boldsymbol{\nabla}T|^2\rangle = \frac{ad}{AD}\left(\frac{2n\tau}{d}\right)^2. \qquad (30)$$

The vertical temperature flux can now be determined from (17):

$$\langle w'T'\rangle = -4\frac{a\kappa_T n^2 \tau^2}{ADd}\left(\frac{dT_0}{dz}\right)^{-1}, \qquad (31)$$

and the corresponding density flux is

$$\langle w'\rho'\rangle = 4\frac{\alpha\rho_0 a\kappa_T n^2 \tau^2}{ADd}\left(\frac{dT_0}{dz}\right)^{-1}. \qquad (32)$$

The rate of potential energy increase can now be determined by inserting (32) in (5). This gives

$$\frac{\partial E_p}{\partial t} = 4a\alpha g\rho_0\kappa_T n^2 \tau^2\left(d\frac{dT_0}{dz}\right)^{-1}, \qquad (33)$$

which is identical with (28). The rate of potential energy increase obtained with the OC model is therefore equal to the rate of background potential energy increase. This is not a rigid proof, but it is a clear indication that the OC model can be used, just as well as the Winters and D'Asaro (1996) model, to determine diapycnal mixing and the corresponding increase in background potential energy in a basin with patchy mixing.

Taking these results into account, the field data in St. Laurent and Schmitt (1999) can be taken as representative for the large-scale flux Richardson number, supporting the value $R_f = 0.11$, mentioned in the introduction.

5. Two apparent paradoxes

Based on the results in the previous sections, one may pose two related, but different apparent paradoxes. Resolving these gives some additional insight into the use and validity of the diascalar mixing expression in (22), and the OC model in (17).

a. Diapycnal flux versus background potential energy

Consider the patch in Fig. 3 but now place it in a basin with the same lateral extension as the patch (see Fig. 4). Since the temperature microstructures are identical in Figs. 3 and 4, the integrated diapycnal flux, $A\varphi_d$, across each isopycnal surface, must also be identical. A quick look at (12) therefore shows that the rate of background potential energy increase must be identical in the two basins. Nevertheless, the results in section 3 shows that the final increase in background potential energy differ by a factor of 2 in the two basins.

The error in the argument above is made in the examination of (12). The diapycnal fluxes across each isopycnal surface are identical in the two patches; that is, the function $A\varphi_d(\rho)$ is identical for the two cases. The vertical positions of the isopycnals after adiabatic redistribution, $z^*(\rho)$, are however different in the two cases, which means that the functions, $A\varphi_d(z^*)$, are different. The increase in background potential energy as obtained from (12) is therefore not identical for the two patches, as illustrated below.

In the small basin (Fig. 4) the mean-squared density gradient within the patch is

$$\langle|\boldsymbol{\nabla}T|^2\rangle_{z^*} = \left(\frac{2n\tau}{d}\right)^2. \qquad (34)$$

The background temperature gradient within the patch is

$$\frac{dT}{dz^*} = \frac{2\tau}{d}. \qquad (35)$$

The diascalar flux of temperature is, from (22), (34), and (35),

$$\varphi_{dT} = -2\kappa_T n^2 \tau d^{-1}, \qquad -\frac{1}{2}d < z^* < \frac{1}{2}d, \quad (36)$$

which gives the diapycnal flux of density

$$\varphi_d = 2\alpha\rho_0\kappa_T n^2 \tau d^{-1}, \qquad -\frac{1}{2}d < z^* < \frac{1}{2}d. \quad (37)$$

From (27) and (37) we get that the horizontally integrated diapycnal fluxes in both the small and large basin can be written as

a)

b)
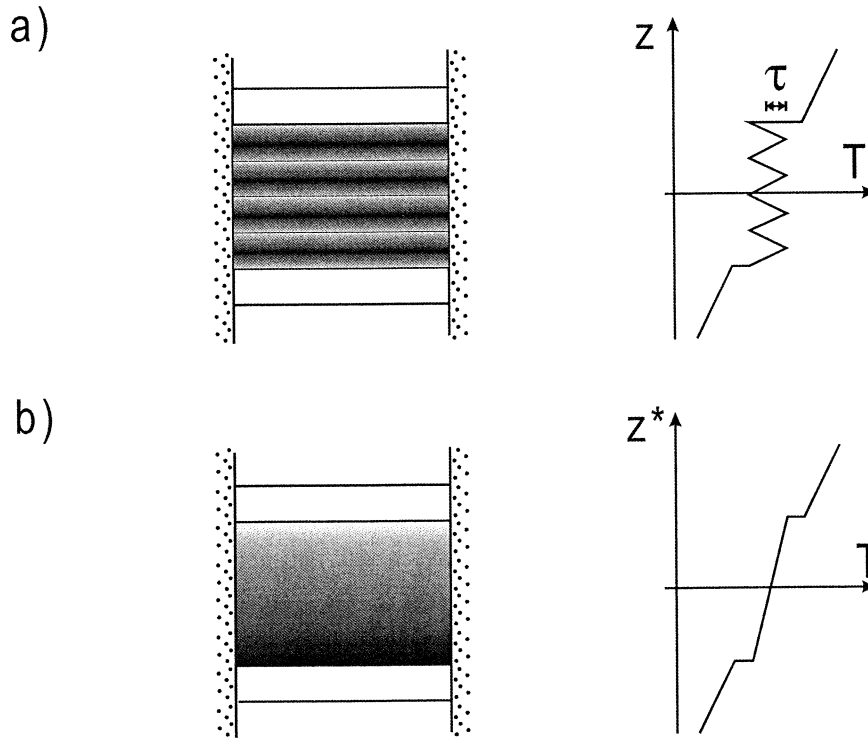
FIG. 4. Patch in a small basin (a) before and (b) after redistribution to state of minimum potential energy.

$$\int \varphi_d \, dA$$

$$= \begin{cases} 2\alpha\rho_0 a\kappa_T n^2 \tau d^{-1}, & T_0(0) - \tau < T < T_0(0) + \tau \\ 0, & \text{elsewhere,} \end{cases}$$

(38)

which shows that the diapycnal fluxes across each isopycnal surface are identical in the two cases, as one would expect.

The rate of background potential energy change in the small basin caused by diapycnal mixing within the patch can be found from (37) and (12). This is

$$\frac{\partial E_b}{\partial t} = 2a\alpha g\rho_0 \kappa_T n^2 \tau. \tag{39}$$

By comparing (39) with (28) it can be seen that the rate of background potential energy increase in the small basin is always larger than the corresponding increase in the large basin except when $\tau = \frac{1}{2}d(dT_0/dz)$, that is, before any diapycnal mixing has taken place. This shows that the two basins have different rates of background potential energy increase even though the diapycnal fluxes across each diapycnal surface are identical in the two basins. The reason is that the isopycnal surfaces are squeezed more together after adiabatic redistribution in the large basin than in the small basin.

b. Using the Osborn and Cox model in a basin with laterally homogeneous mixing

The second apparent paradox is obtained by using the OC model to determine the vertical buoyancy flux in the small basin in Fig. 4. As will be shown below, the OC model gives no difference between the horizontally integrated vertical buoyancy flux in the large and in the small basin. One may see this by direct inspection of (17) since both the volume-average vertical temperature gradients and the horizontally integrated temperature gradient variances are identical in the two basins. By inserting these buoyancy fluxes in (5) and integrating over time, one obtains that the potential energy increases are identical in the two basins. This is in conflict with the results above, which show that the potential energy increase in the small basin is twice the potential energy increase in the large basin. In section 4 it was shown that the OC model and the diascalar flux model (22) gave identical results in the large basin. Remaining are the possibilities that the OC model underestimates the vertical buoyancy flux in the small basin, or that the results above are wrong. It will be explained below why the OC model is wrong in the small basin, but first I will show that the model gives identical fluxes in the two basins.

Using the same averaging volume (with thickness $D > d$) as in section 4, it is found that the average vertical temperature gradient is equal to the expression in (29)

FIG. 5. Evolution of temperature variance in a (a) small and (a′) large basin, time-integrated vertical temperature-variance flux in a (b) small and large (b′) basin, and (c) negative dissipation of temperature variance. States A, B, and C are also shown.

and that the average temperature gradient variance is given by

$$\langle |\nabla T|^2 \rangle = \frac{d}{D}\left(\frac{2n\tau}{d}\right)^2. \tag{40}$$

As in section 4 the temperature flux can be obtained from (17), the buoyancy flux by multiplying the temperature flux with $-\alpha\rho_0$, and the rate of potential energy increase by inserting the buoyancy flux in (5). The result is

$$\frac{\partial E_p}{\partial t} = 4a\alpha g\rho_0\kappa_T n^2\tau^2\left(d\frac{dT_0}{dz}\right)^{-1}, \tag{41}$$

which is identical with (33). This means that the OC model is not able to differ between the small and the large basin.

The reason why the OC model underestimates the buoyancy flux in the small basin can be found by inspecting the temperature variance equation. In this case the three relevant terms are

$$\left\langle\frac{\partial T'^2}{\partial t}\right\rangle + 2\langle w'T'\rangle\left\langle\frac{\partial T}{\partial z}\right\rangle = -\chi. \tag{42}$$

Integration of (42) with respect to time gives

$$\langle T'(t)^2\rangle + 2\frac{\partial T_0}{\partial z}\int_A^t \langle w'T'\rangle\, dt = -\int_A^t \chi\, dt. \tag{43}$$

$$\underset{(a)}{} \qquad\qquad \underset{(b)}{} \qquad\qquad \underset{(c)}{}$$

The time-integrated contributions from each of these terms during a mixing event are sketched in Fig. 5. During the initial turbulent mixing of a patch, the dissipation of temperature variance, (c), is small relative to the other terms, which means that the production of temperature variance by turbulent fluctuations, (b), is balanced by the increase

in temperature variance, (a). Gradually the dissipation becomes larger than the production, and the new balance is between the dissipation and a decrease in temperature variance. Finally, at state B, the dissipation ceases because there is no more temperature gradient variance. The temperature variance is, however, not zero at state B, as one might expect. The temperatures within the homogeneous patch deviate from the "average" or large-scale temperature profile $T_0(z)$, and therefore the temperature variance is different from zero. The volume-average temperature variance at state B is

$$\langle T'^2\rangle = \frac{a}{AD}\int_{-d/2}^{d/2}\left(-z\frac{dT_0}{dz}\right)^2 dz = \frac{1}{12}\frac{ad^3}{AD}\left(\frac{dT_0}{dz}\right)^2. \tag{44}$$

Between state A and B vertical transports of temperature are caused by turbulent advective transports only (the *vertical* transports by molecular *diascalar* fluxes are negligible). The vertical transports through level $z = -d/2$ is zero. The vertical transports of temperature, integrated horizontally and in time from state A to state B are therefore distributed with depth as

$$\iint_A^B w'T'\, dt\, dA = -a\int_{-d/2}^z \Delta T\, dz$$

$$= -\frac{1}{2}\frac{dT_0}{dz}\left(z^2 - \frac{1}{4}d^2\right). \tag{45}$$

After integrating (45) with respect to z and dividing with the integration volume, the following expression for the volume-average, time-integrated, vertical temperature flux is obtained:

$$\int_A^B \langle w'T'\rangle\, dt = -\frac{1}{12}\frac{ad^3}{AH}\frac{dT_0}{dz}. \tag{46}$$

By use of (46) and (44) we now see that the value of term (a) in (43) is minus half the value of term (b) at state B.

In a large basin, state B will be followed by a collapse, during which there is a balance between terms (a) and (b), so that the remaining temperature variance disappears, while the time-integrated temperature flux is halved. In that case the OC model is correct because there is a long-term balance between the time- and volume-averaged production of temperature variance (b) and the dissipation of temperature variance (c). In the small basin, however, state B is the final state, in which the temperature variance can not be neglected, and this is the reason why the temperature flux is underestimated with a factor of two in the OC model.

6. Summary and discussion

In the present paper, it has been shown that it is possible to define two different flux Richardson numbers for mixing in a system with patchy and intermittent turbulence. One, the small-scale flux Richardson number, R_{f_t}, is characteristic for the small-scale tur-
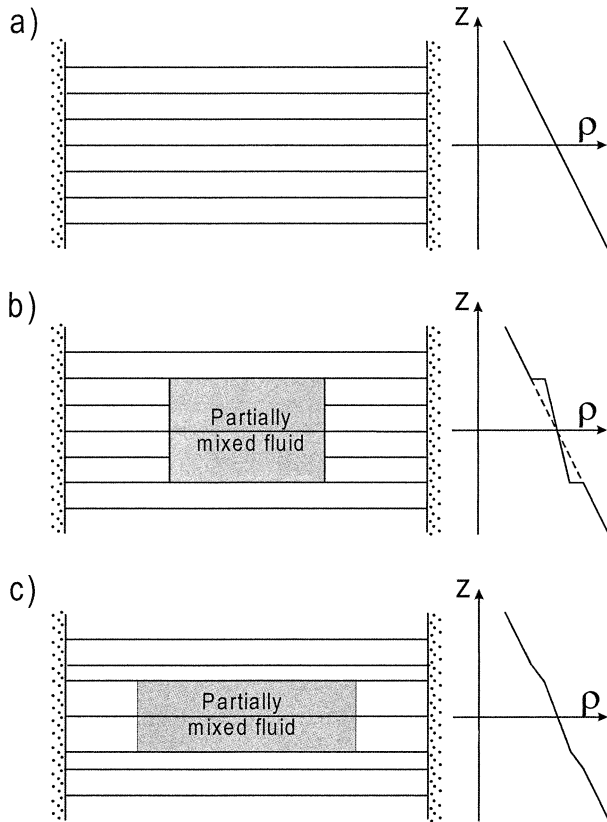
FIG. 6. Vertical section and density profile through (a) a linearly stratified basin (state A), (b) the same basin after partial mixing of a patch (state B), and (c) after the partially mixed fluid has spread out and obtained static equilibrium with the surrounding water (state C).

bulent mixing within the patches. This is the parameter that is obtained from laboratory and numerical experiments intended to determine turbulent mixing efficiencies. The other, the large-scale flux Richardson number, R_f, is the relevant parameter in order to determine large-scale, irreversible, changes in the stratification caused by mixing. One may say that R_{ft} is a process parameter that only describes the particular process of turbulent mixing, while R_f is a system parameter that describes changes in the system caused by turbulent mixing and redistribution of the mixed fluid following the mixing.

The large-scale flux Richardson number is always smaller than the small-scale flux Richardson number. The reason is that some of the initial gain in potential energy by turbulent mixing within the patch is lost in the subsequent collapse of the mixed patch. If the patch is homogenized totally, half of the potential energy is lost during the collapse. This was noted by Garrett (1984) but has, to my knowledge, not previously been used in a discussion about mixing efficiencies.

I argue that mixing efficiencies obtained from past laboratory and numerical experiments represent the small-scale mixing efficiency rather than the large-scale mixing efficiency. This means that one should use down

to half the value rather than the actual value when taking mixing efficiency results from laboratory experiments and applying them in a patchy system. Past laboratory and numerical experiments indicate a maximum small-scale flux Richardson number, $R_{ft} = 0.2$. Taking into account the loss of potential energy by collapsing patches in a patchy system, this corresponds to a large-scale flux Richardson number $R_f = 0.11$.

Turbulence in the interior of oceans, lakes, and fjords is highly intermittent and patchy. I therefore propose that the value $R_f = 0.11$ should be used for these systems. This is considerably smaller than the values $R_f = 0.17$–0.2, used by the majority of oceanographers today. The lower value is, however, supported by the field results in St. Laurent and Schmitt (1999), where the average flux Richardson number for active turbulence under double-stable conditions is $R_f = 0.11$. These results are based on microstructure temperature and velocity data, and the buoyancy flux has been estimated, using the OC model.

By comparison of the OC model with the diascalar flux expression derived in Winters and D'Asaro (1996), I show that the OC model can be expected to work in a patchy system. It does not work, however, in a system where mixing is laterally uniform over a whole basin but confined vertically to a patch. The reason is that the increase in temperature variance for such a system can not be neglected in the temperature variance equation as it is in the OC model.

A factor of 2 in error for the mixing efficiency may not seem very large. Such an error may though lead to large errors in, for example, energy budgets of abyssal mixing in the oceans. Munk and Wunsch (1998) estimated the work needed to balance 30 Sv upwelling at 1000 m. They found that a power of 2.1 TW was needed, using a flux Richardson number, $R_f = 0.2$, and ocean-averaged stratification data. Using $R_f = 0.11$ instead means that one should look for global energy sources in the order of 3.8 TW, rather than 2.1 TW. The tidal contribution (0.9 TW) is relatively well known, so left is the wind contribution which should be in the order of 2.9 TW rather than 1.2 TW, quite a different number! Alternatively the mixing needed to balance the upwelling is overestimated. Sjöberg and Stigebrandt (1992) were able to balance 15 Sv upwelling at 1000-m depth with 1.3 TW and a flux Richardson number, $R_f = 0.056$, using stratification data from a $1° \times 1°$ database. For comparison the energy required to balance 30 Sv would then be 1.32 TW, using the same stratification data but $R_f = 0.11$. Using the latter number in Munk and Wunsch's budget gives a wind contribution, which is half the tidal contribution. All these numbers are very uncertain, but they illustrate the difference a factor of 2 can make. They also illustrate the need for further investigations on the horizontal variations of vertical mixing—on small and large scales.

have lead to considerable improvements of the manuscript. I also want to thank Anders Stigebrandt for helpful comments and suggestions.

APPENDIX

Partly Mixed Patch

Assume that the turbulent mixing has only partly homogenized the patch so that the stratification at state B looks like in Fig. 6. This case was solved in Hebert (1988) but was used for the calculation of available potential energies in eddies rather than for mixing considerations.

The change in potential energy from state A to state B can be found to be

$$\Delta E_{pAB} = \frac{1}{12}\rho_0(N_0^2 - N_p^2)d^3a, \qquad (A1)$$

where N_p is the buoyancy frequency inside the patch at state B. As one would expect, (A1) is identical with (3) for $N_p = 0$, while the potential energy change is 0 for $N_p = N_0$.

After collapse of the patch, the stratification looks like sketched in Fig. 6b. Thus, the mixed fluid does not have to be spread out into the whole basin to obtain gravitational equilibrium. When spreading out horizontally the vertical density gradient increases within the patch. The surrounding fluid located within the same isopycnals as the fluid in the patch is compressed horizontally and therefore expanded vertically. This decreases the density gradient. Equilibrium is obtained when the two gradients are equal, which happens when the horizontal patch area is

$$a' = \frac{aAN_0^2}{AN_p^2 + a(N_0^2 - N_p^2)}. \qquad (A2)$$

The final difference in potential energy from state A to state C is

$$\Delta E_{pAC} = \frac{1}{24}\rho_0(N_0^2 - N_p^2)d^3a\left[1 + \frac{a}{A} + \frac{N_p^2}{N_0^2}\left(1 - \frac{a}{A}\right)\right]. \qquad (A3)$$

The potential energies at state B and C are related through

$$\Delta E_{pAC} = \frac{1}{2}\left[1 + \frac{a}{A} + \frac{N_p^2}{N_0^2}\left(1 - \frac{a}{A}\right)\right]\Delta E_{pAB}. \qquad (A4)$$

For N_p^2 approaching zero (total mixing), (A3) is identical with (4), which means that the background flux Richardson number is only half the small-scale flux Richardson number if the patch is small relative to the reference volume. For N_p^2 approaching N_0^2 the fraction of potential energy at state B, which is lost during the collapse, is reduced.

REFERENCES

Arneborg, L., and B. Liljebladh, 2001: The internal seiches in Gullmar Fjord. Part II: Contribution to basin water mixing. *J. Phys. Oceanogr.,* **31,** 2567–2574.

De Silva, I. P. D., and H. J. S. Fernando, 1998: Experiments on collapsing turbulent regions in stratified fluids. *J. Fluid Mech.,* **358,** 29–60.

Garrett, C., 1984: Turning points in universal speculation on internal waves. *A Celebration in Geophysics and Oceanography,* C. Garrett and C. Wunsch, Eds., Scripps Reference Series, Vol. 84, 38–46.

——, 1991: Marginal mixing theories. *Atmos.–Ocean.,* **29,** 313–339.

Gregg, M. C., 1998: Estimation and geography of diapycnal mixing in the stratified ocean. *Physical Processes in Lakes and Oceans,* J. Imberger, Ed., Amer. Geophys. Union, 305–338.

Hebert, D., 1988: The available potential energy of an isolated feature. *J. Geophys. Res.,* **93,** 556–564.

Imberger, J., and G. N. Ivey, 1991: On the nature of turbulence in a stratified fluid. Part II: Application to lakes. *J. Phys. Oceanogr.,* **21,** 659–680.

Inall, M. E., T. P. Rippeth, and T. J. Sherwin, 2000: Impact of nonlinear waves on the dissipation of internal tidal energy at a shelf break. *J. Geophys. Res.,* **105,** 8687–8705.

Itsweire, E. C., J. R. Koseff, D. A. Briggs, and J. H. Ferziger, 1993: Turbulence in stratified shear flows: Implications for interpreting shear-induced mixing in the ocean. *J. Phys. Oceanogr.,* **23,** 1508–1522.

Ivey, G. N., and J. Imberger, 1991: On the nature of turbulence in stratified fluid. Part I: The energetics of mixing. *J. Phys. Oceanogr.,* **21,** 650–658.

Ledwell, J. R., E. T. Montgomery, K. L. Polzin, L. C. St. Laurent, R. W. Schmitt, and J. M. Toole, 2000: Evidence for enhanced mixing over rough topography in the abyssal ocean. *Nature,* **403,** 179–182.

Lemckert, C. J., and J. Imberger, 1993: Axisymmetric intrusive gravity currents in linearly stratified fluids. *J. Hydrol. Eng.,* **119,** 662–679.

Linden, P. F., 1979: Mixing in srtified fluids. *Geophys. Astrophys. Fluid. Dyn.,* **13,** 3–23.

Munk, W., and C. Wunsch, 1998: Abyssal recipes II: Energetics of tidal and wind mixing. *Deep-Sea Res. I,* **45,** 1977–2010.

Osborn, T. R., and C. S. Cox, 1972: Oceanic fine structure. *Geophys. Fluid Dyn.,* **3,** 321–346.

Piccirillo, P., and C. W. Van Atta, 1997: The evolution of uniformly sheared thermally stratified turbulent flow. *J. Fluid Mech.,* **334,** 61–86.

Rohr, J. J., E. C. Itsweire, and C. W. Van Atta, 1984: Mixing efficiency in stably stratified decaying turbulence. *Geophys. Astrophys. Fluid. Dyn.,* **29,** 221–236.

Ruddick, B., D. Walsh, and N. Oakey, 1997: Variations in apparent mixing efficiency in the North Atlantic Central Water. *J. Phys. Oceanogr.,* **27,** 2589–2605.

Sjöberg, B., and A. Stigebrandt, 1992: Computations of the geographical distribution of the energy flux to mixing processes via internal tides and the associated vertical circulation in the ocean. *Deep-Sea Res.,* **39,** 269–291.

Stigebrandt, A., 1999: Resistance to barotropic tidal flow in straits by baroclinic wave drag. *J. Phys. Oceanogr.,* **29,** 191–197.

St. Laurent, L., and R. W. Schmitt, 1999: The contribution of salt fingers to vertical mixing in the North Atlantic Trace Release Experiment. *J. Phys. Oceanogr.,* **29,** 1404–1424.

Thorpe, S. A., 1999: On internal wave groups. *J. Phys. Oceanogr.,* **29,** 1085–1095.

Winters, K. B., and E. A. D'Asaro, 1996: Diascalar flux and the rate of fluid mixing. *J. Fluid. Mech.,* **317,** 179–193.

——, P. N. Lombard, J. J. Riley, and E. A. D'Asaro, 1995: Available potential energy and mixing in density-stratified fluids. *J. Fluid Mech.,* **289,** 115–128.